RSC Advances

PAPER

View Article Online
View Journal | View Issue

Cite this: *RSC Adv.*, 2015, **5**, 41401

The importance of Au···π(aryl) interactions in the formation of spherical aggregates in binuclear phosphane gold(I) complexes of a bipodal thiocarbamate dianion: a combined crystallographic and computational study, and anti-microbial activity†

Chien Ing Yeo,[a] Chai-Hoon Khoo,[b] Wern-Cui Chu,[b] Bao-Jing Chen,[b] Pek-Lim Chu,[b] Jiun-Horng Sim,[b] Yoke-Kqueen Cheah,*[b] Jimmy Ahmad,[a] Siti Nadiah Abdul Halim,[a] Hoi-Ling Seng,[c] Soon Ng,[a] A. Otero-de-la-Roza*[d] and Edward R. T. Tiekink*[a]

Binuclear phosphanegold(I) complexes of a bipodal thiocarbamate dianion, $(R_3PAu)_2L$, R = Et (**1**), Ph (**2**) and Cy (**3**), where LH_2 is {1,4-[MeOC(=S)N(H)]$_2$C$_6$H$_4$}, have been synthesised, and characterised spectroscopically (NMR and IR) and by X-ray crystallography. The gold atoms are linearly coordinated within a *P*-,*S*-donor set, and are oriented toward the central ring to form intramolecular Au···π(aryl) interactions, rather than the intramolecular Au···O interactions normally observed in mononuclear analogues. This phenomenon has been investigated by theory (LC-ωPBE-XDM) for **1** which revealed that the geometry optimised species with two Au···π(aryl) interactions is more stable by at least 12 kcal mol^{-1} compared to conformations having one or more Au···O interactions instead. The disk diffusion, minimum inhibitory concentration (MIC) and minimum bactericidal concentration (MBC) methods were used to observe the inhibitory effect of complexes **1**–**3**. The disk diffusion results demonstrated that **1** exhibited a broad spectrum of anti-bacterial activity toward 24 strains of Gram-positive and Gram-negative bacteria. By contrast, the anti-bacterial activity of **2** and **3** was limited to Gram-positive bacteria. Further evaluation showed that **1** exhibited marked bactericidal activity against *B. cereus*, *B. subtilis*, *E. faecalis*, *L. monocytogenes*, *S. aureus*, *S. saprophyticus* and methicillin resistant *S. aureus cf.* standard antibiotics tetracycline and chloramphenicol.

Received 30th March 2015
Accepted 21st April 2015

DOI: 10.1039/c5ra05604g

www.rsc.org/advances

Introduction

The structural diversity and the fascinating architectures they sustain have ensured that aurophilic (Au···Au) interactions have garnered the attention of chemists for decades.[1] The aggregation of gold compounds in this fashion arises from relativistic effects which are at a maximum for gold compared to other heavy elements.[2] Over and above aesthetics, interest in gold compounds/aurophilic interactions stems from their luminescence properties, in both the solid-state and in solution.[3] By contrast to aurophilic interactions, the recognition of supramolecular association based on Au···π(aryl) interactions is still in its infancy,[4a] despite them being often crucial in the reaction mechanisms related to the burgeoning field of gold-based catalysis.[5] It is only in recent years that bibliographic surveys have shown that Au···π(aryl) interactions provide readily identifiable points of contact between molecules in their crystal structures, operating in isolation of other supramolecular synthons.[4]

The themes of aurophilic and Au···π(aryl) interactions as well as luminescence feature prominently in the chemistry of phosphanegold(I) thiocarbamates, where the thiolate anion is derived from thiocarbamide molecules of the general formula RN(H)C(=S)OR′, R,R′ = alkyl and/or aryl.[6] In the overwhelming majority of crystal structures of phosphanegold(I) thiocarbamates, the thiolate ligand is oriented so that the oxygen

[a]*Department of Chemistry, University of Malaya, 50603 Kuala Lumpur, Malaysia. E-mail: Edward.Tiekink@gmail.com*

[b]*Department of Biomedical Science, Faculty of Medicine and Health Sciences, University Putra Malaysia, 43400 Serdang, Selangor Darul Ehsan, Malaysia. E-mail: ykcheah@medic.upm.edu.my*

[c]*Department of Biological Sciences, Faculty of Science and Technology, Sunway University, 47500 Bandar Sunway, Selangor Darul Ehsan, Malaysia*

[d]*National Institute for Nanotechnology, National Research Council of Canada, 11421 Saskatchewan Drive, Edmonton, Alberta, Canada T6G 2M9. E-mail: alberto.oterodelaroza@nrc-cnrc.gc.ca*

† Electronic supplementary information (ESI) available. CCDC 1041500–1041502. For ESI and crystallographic data in CIF or other electronic format see DOI: 10.1039/c5ra05604g

atom is located in close proximity to the gold atom. However, by careful choice of R and R′ substituents of the thiolate anion and by using isomeric tolylphosphane ligands, it proved possible to orient the thiolate so that the aryl ring was proximate to the gold atom instead.[6c] Crystal engineering considerations notwithstanding, phosphanegold(I) thiocarbamates also exhibit promising biological activity.

Gold(I) compounds are used clinically in the treatment of severe forms of rheumatoid arthritis, being a member of the disease modifying anti-rheumatic drugs (DMARDS) class of anti-arthritic agents.[7a–c] Spurred by the observation that patients undergoing *chrysotherapy*, appeared to suffer reduced rates of malignant disease,[7d] both gold(I) and gold(III) compounds are under intense investigation as potential anti-tumour drugs.[8] In the context of the present study, phosphanegold(I) thiocarbamates of the general formula $Ph_3PAu[SC(OR)=NPh]$, R = Me, Et and iPr, exhibit significant cytotoxicity toward HT-29 colon cancer cells, have been shown to function through both intrinsic and extrinsic apoptotic pathways, and to be topoisomerase I inhibitors.[9] Gold compounds are also under active evaluation as anti-microbial agents.[10] Recently, another series of phosphanegold(I) thiocarbamates, namely $Ph_3PAu[SC(OR)=N(p\text{-tol})]$, R = Me, Et and iPr, have proven to be very effective against a panel of Gram-positive bacteria.[11]

It was primarily the biological context that led to the synthesis of the title binuclear compounds, $(R_3PAu)_2L$, R = Et (**1**), Ph (**2**) and Cy (**3**), where LH_2 is the bipodal molecule {1,4-$[MeOC(=S)N(H)]_2C_6H_4$}. Herein, their characterization, including by X-ray crystallography and Density Functional Theory (DFT) calculations is described along with an evaluation of their potential anti-microbial activity.

Experimental section

Materials, methods and Instruments

All chemicals and solvents were used as purchased without purification. All reactions were carried out under ambient conditions. Elemental analyses were performed on a Perkin Elmer PE 2400 CHN Elemental Analyser. Melting points were determined on a Krüss KSP1N melting point meter. ^1H and $^{13}C\{^1H\}$ NMR spectra were recorded in both DMSO-d_6 and $CDCl_3$ solutions for LH_2, and $CDCl_3$ solutions for 1–3 on a Bruker Avance 400 MHz NMR spectrometer with chemical shifts relative to tetramethylsilane. $^{31}P\{^1H\}$ NMR spectra were recorded in $CDCl_3$ solution on the same instrument but with the chemical shifts recorded relative to 85% aqueous H_3PO_4 as the external reference; abbreviations for NMR assignments: s, singlet; d, doublet; m, multiplet; dq, doublet of quartets; dt, doublet of triplets. For the relaxation experiments on **1**, a solution of the compound (20 mg) was prepared in $CDCl_3$ (4.5 cm) in a 5 mm NMR tube (Wilmad). The solution was degassed through five freeze–pump–thaw cycles and sealed under vacuum. The NMR measurements were carried out on a JEOL ECX500 NMR spectrometer. The ^{13}C spin–lattice relaxation time (T_1) was obtained by using the two-pulse inversion–recovery (IR) method.[12] Initially, an approximate T_1 value was obtained before a more precise measurement was made using 10 IR intervals in a range up to $1.5T_1$. Subsequently, a final measurement was made to confirm the value T_1 = 0.69 s at 20 °C. Then, the NOE measurements were made in two consecutive experiments: one with complete proton decoupling with a relaxation delay of 6.0 s and an acquisition time of 1.04 s, and the other experiment with gated-decoupling in which the NOE was suppressed but with the remaining conditions the same as in the first experiment. The pulse angle was 90°. Good signal intensity was obtained with 1024 scans. The total integrated intensity of the signal was obtained with the spectrometer's data processing software. The ratio of the signal intensities in the two experiments gives the NOE value, usually given as NOE = 1 + η, where η is the NOE enhancement factor. IR spectra were measured on a Perkin Elmer Spectrum 400 FT Mid-IR/Far-IR spectrophotometer from 4000 to 400 cm^{-1}; abbreviations: vs, very strong; s, strong; m, medium; br, broad. Thermogravimetric analyses were performed on a Perkin Elmer TGA 4000 Thermogravimetric Analyzer in the range of 35–850 °C at the rate of 10 °C min^{-1}. Powder X-ray diffraction (PXRD) data were recorded with a PANalytical Empyrean XRD system with Cu-Kα1 radiation (λ = 1.54056 Å) in the 2θ range 5 to 50°. The comparison between experimental and calculated (from CIF's) PXRD patterns were performed with X'Pert HighScore Plus.[13]

Synthesis of LH_2. LH_2 was prepared in similar manner as described in the literature for mono-functional analogues[14] whereby *p*-phenylene diisothiocyanate (2.50 mmol, 0.48 g; Sigma-Aldrich) was reacted in MeOH (100 ml) in the presence of two mole equivalents of NaOH, yielding a pale-yellow powder. Yield: 0.596 g (93%). mp 209.0–210.0 °C. Anal. calc. for $C_{10}H_{12}N_2O_2S_2$: C, 46.85; H, 4.72; N, 10.93. Found: C, 46.71; H, 4.64; N, 10.94%. IR (ν, cm^{-1}): 3219 (*br*) ν(N–H), 1454 (s) ν(C–N), 1140 (s) ν(C–O), 1046 (s) ν (C=S). ^1H NMR (DMSO-d_6): δ 11.10 [s, br, 2H, NH], 7.59 [s, br, 2H, aryl-H], 7.30 [s, br, 2H, aryl-H], 3.99 [s, 6H, OCH_3] ppm. ^1H NMR (CDCl3): δ 8.32 [s, br, 2H, NH], 7.56 [s, br, 2H, aryl-H], 7.22 [s, br, 2H, aryl-H], 4.12 [s, 6H, OCH_3] ppm. $^{13}C\{^1H\}$ NMR (DMSO-d_6): δ 189.1, 188.4 [C_q], 135.8, 134.8 [C_{ipso}], 123.7 and 122.6 [C_{ortho}], 58.3, 56.8 [OCH_3] ppm.

Synthesis of $(R_3PAu)_2L$, R = Et (1), Ph (2) and Cy (3). The methods employed for the preparation and recrystallization of **1–3** were similar, so the preparation of the Et_3P derivative (**1**) is described in detail as a representative example. The R_3PAuCl, R = Et, Ph and Cy, precursors employed in the synthesis were prepared following standard procedures by reducing $KAuCl_4$ (Sigma-Aldrich) using one mole excess sodium sulfite (Merck), and then further reacted with one mole equivalent of either Et_3P (Merck), Ph_3P (Merck) or Cy_3P (Sigma-Aldrich), to yield the respective precursor.

$(Et_3PAu)_2L$ (1). NaOH (0.50 mmol) in water (5 ml) was added to a suspension of Et_3PAuCl (0.50 mmol) in acetonitrile (20 ml) followed by addition of LH_2 (0.25 mmol) in acetonitrile (20 ml). The resulting mixture was stirred for 3 h at 50 °C. Extraction followed with dichloromethane (100 ml) and an equivalent volume of acetonitrile added. The solution was left for slow evaporation at room temperature, giving colourless crystals after 2 weeks. Yield: 0.206 g (93%). mp 174.0–176.0 °C. Anal. calc. for $C_{22}H_{40}Au_2N_2O_2P_2S_2$: C, 29.87; H, 4.56; N, 3.17. Found: C, 29.92; H, 4.53; N, 3.04%. IR (cm^{-1}): 1421 (m) ν(C=N),

1123 (vs) ν(C–O), 1094 (s) ν(C–S). ^{1}H NMR ($CDCl_3$): δ 6.72 [s, 4H, aryl-H], 3.81 [s, 6H, OCH_3], 1.70 [dq, 12H, CH_2P, $^3J_{HH} = 7.75$, $^2J_{PH} = 9.82$ Hz], 1.06 [dt, 18H, CH_3CH_2P, $^3J_{HH} = 7.62$, $^3J_{PH} = 18.32$ Hz] ppm. $^{13}C\{^1H\}$ NMR ($CDCl_3$): δ 165.3 [C_q], 145.7 [aryl, C_{ipso}], 122.8 [aryl, C_{ortho}], 55.2 [OCH_3], 17.6 [d, CH_2P $^1J_{CP} = 33.3$ Hz], 8.8 [s, CH_3CH_2P] ppm. $^{31}P\{^1H\}$ NMR ($CDCl_3$): δ 35.6 ppm.

$(Ph_3PAu)_2L$ (2). A similar synthetic procedure as employed for **1** was used for the synthesis of **2** except that the gold precursor was replaced by Ph_3PAuCl. Colourless crystals. Yield: 0.255 g (87%). mp 181.5–183.0 °C. Anal. calc. for $C_{46}H_{40}Au_2N_2O_2P_2S_2$: C, 47.11; H, 3.44; N, 2.39. Found: C, 47.25; H, 3.31; N, 2.41%. IR (cm^{-1}): 1434 (s) ν(C=N), 1143 (s) ν(C–O), 1101 (s) ν(C–S). ^{1}H NMR ($CDCl_3$): δ 7.49–7.41 [m, 30H, Ph_3P], 6.41 [s, 4H, aryl-H], 3.73 [s, 6H, OCH_3] ppm. $^{13}C\{^1H\}$ NMR ($CDCl_3$): δ 163.2 [C_q], 145.7 [aryl, C_{ipso}], 134.4 [d, *o*-Ph_3P, $^2J_{CP} = 13.9$ Hz], 131.4 [d, *p*-Ph_3P, $^4J_{CP} = 2.2$ Hz], 129.6 [d, i-Ph_3P, $J_{CP} = 57.0$ Hz], 128.9 [d, *m*-Ph_3P, $^3J_{CP} = 11.5$ Hz], 122.4 [aryl, C_{ortho}], 55.0 [OCH_3] ppm. $^{31}P\{^1H\}$NMR ($CDCl_3$): δ 38.1 ppm.

$(Cy_3PAu)_2L$ (3). The synthesis was as for **1** but using Cy_3PAuCl. Colourless crystals. Yield: 0.275 g (91%). mp 180.0–181.0 °C. Anal. calc. for $C_{46}H_{76}Au_2N_2O_2P_2S_2$: C, 45.69; H, 6.34; N, 2.32. Found: C, 45.57; H, 6.40; N, 2.24%. IR (cm^{-1}): 1444 (s) ν(C=N), 1130 (s) ν(C–O), 1093 (m) ν(C–S). ^{1}H NMR ($CDCl_3$): δ 6.84 [s, 4H, aryl-H], 3.82 [s, 6H, OCH_3], 1.98–1.20 [m, 66H, Cy_3P] ppm. $^{13}C\{^1H\}$ NMR ($CDCl_3$): δ 163.9 [C_q], 145.4 [aryl, C_{ipso}], 122.4 [aryl, C_{ortho}], 54.8 [OCH_3], 33.3 [d, 1-Cy_3P, $J_{CP} = 27.8$ Hz], 30.7 [s, 3-Cy_3P], 27.0 [d, 2-Cy_3P, $^3J_{CP} = 11.9$ Hz], 25.9 [s, 4-Cy_3P] ppm. $^{31}P\{^1H\}$NMR ($CDCl_3$): δ 56.5 ppm.

X-ray data collection and structure determination

Intensity data were measured at 100 K on an Agilent Technologies SuperNova Dual CCD with an Atlas detector fitted with Mo Kα radiation (λ = 0.71073 Å). Data processing and absorption correction were accomplished with CrysAlis PRO.[15a] With the use of SHELX programs[15b] integrated into WinGX,[15c] the structures were solved by direct methods and refined on F^2 by full-matrix least-squares with anisotropic displacement parameters for all non-hydrogen atoms. The C-bound H atoms were placed on stereochemical grounds and refined in the riding model approximation with $U_{iso} = 1.2–1.5U_{eq}$(carrier atom). A weighting scheme of the form $w = 1/[\sigma^2(F_o^2) + (aP)^2 + bP]$ where $P = (F_o^2 + 2F_c^2)/3$ was introduced in each case. For **1**, the residual electron density peaks were located 0.95 and 0.96 from the Au atom, and for **2**, the peaks were 0.90 and 0.86 from the Au atom. Details of cell data, X-ray data collection and structure refinement are given in Table 1. The programs ORTEP-3 for Windows,[15c] PLATON,[15d] DIAMOND[15e] and QMol[15f] were also used in the analysis.

Powder X-ray diffraction

Powder X-ray patterns (PXRD) measured on the bulk material for each of **1–3** were compared with the simulated patterns calculated based on the CIF's obtained for the experimental crystal structures.[13] There is a high agreement between the patterns, ESI Fig. S1,† suggesting the single crystal results are representative of the bulk materials.

Computational study

The calculations were run using Gaussian09 (ref. 16) and the LC-ωPBE[17] functional combined with the exchange-hole dipole moment (XDM) model dispersion correction,[18–20] implemented in the postg program.[21] In a previous contribution, it was shown that LC-ωPBE-XDM gives excellent performance in the treatment of aurophilicity,[22] so it is a reasonable choice to study interactions involving gold. Three conformations were examined for **1**: (i) the same conformation as in the crystal structure, with two Au···π(aryl) contacts, (ii) a mixed conformation with one Au···π(aryl) and one Au···O contact, *i.e.* where one Au···π(aryl) interaction of the experimental structure was replaced by a contact between gold and a thiocarbamate-O atom, and (iii) the fully extended, rod-like conformations with two Au···O interactions. The geometry of each conformer was relaxed using the 6-31+G* basis set for all s- and p-block elements and aug-cc-pVDZ-PP scalar relativistic pseudo-potential and basis set combination for Au.[23] Despite the modest size of this basis set, it has been shown in previous work that just one set of diffuse and polarization functions is sufficient to model non-covalent interactions with an accuracy relatively close to the basis-set limit.[24]

Anti-microbial assay

Bacterial strains. The standard reference strains of bacteria used in the present study were *Aeromonas hydrophila* (*A. hydrophila*) ATCC 35654, *Acinetobacter baumannii* (*A. baumannii*) ATCC 19606, *Bacillus cereus* (*B. cereus*) ATCC 10876, *Bacillus subtilis* (*B. subtilis*) ATCC 6633, *Citrobacter freundii* (*C. reundii*) ATCC 8090, *Enterobacter cloacae* (*E. cloacae*) ATCC 35030, *Enterobacter aerogenes* (*E. aerogenes*) ATCC 13048, *Enterococcus faecalis* (*E. faecalis*) ATCC 29212, *Enterococcus faecium* (*E. faecium*) ATCC 19434, *Escherichia coli* (*E. coli*) ATCC 25922, *Klebsiella pneumoniae* (*K. pneumoniae*) ATCC 700603, *Listeria monocytogenes* (*L. monocytogenes*) ATCC 19117, *Proteus mirabilis* (*P. mirabilis)* ATCC 25933, *Proteus vulgaris* (*P. vulgaris*) ATCC 13315, *Pseudomonas aeruginosa* (*P. aeruginosa*) ATCC 27853, *Salmonella paratyphi* A (*S. paratyphi* A) ATCC 9150, *Salmonella typhimurium* (*S. typhimurium*) ATCC 14028, *Shigella flexneri* (*S. flexneri*) ATCC 12022, *Shigella sonnei* (*S. sonnei*) ATCC 9290, *Staphylococcus aureus* (*S. aureus*) ATCC 25923, methicillin resistant *Staphylococcus aureus* (MRSA) ATCC 43300, *Staphylococcus saprophyticus* (*S. saprophyticus*) ATCC 15305, *Stenotrophomonas maltophilia* (*S. maltophilia*) ATCC 13637 and *Vibrio parahaemolyticus* (*V. parahaemolyticus*) ATCC 17802. All bacterial strains were purchased from the American Type Culture Collection (ATCC, Manassas, VA, USA).

Anti-bacterial activity. The anti-bacterial activity of **1–3** was evaluated using the Kirby–Bauer disc diffusion method in accordance with the National Committee for Clinical Laboratory Standards (NCCLS) guidelines. The bacterial cultures were adjusted to 0.5 McFarland standard turbidity (which corresponds to approximately 10^8 CFU ml^{-1}) by adding Mueller-Hinton broth (Difco, USA). This suspension was then swabbed onto the surface of Mueller-Hinton agar (Difco, USA) plates. The tested compounds were dissolved in DMSO to a test concentration of 2 mg ml^{-1}. Sterile 6 mm filter paper discs were

Table 1 Crystal data, data collection and refinement parameters for compounds 1–3

	1	2	3
Formula	$C_{22}H_{40}Au_2N_2O_2P_2S_2$	$C_{46}H_{40}Au_2N_2O_2P_2S_2$	$C_{46}H_{76}Au_2N_2O_2P_2S_2$
Formula weight	884.56	1172.79	1209.08
Crystal size (mm)	0.10 × 0.20 × 0.25	0.20 × 0.20 × 0.30	0.20 × 0.30 × 0.30
Crystal system	Monoclinic	Triclinic	Monoclinic
Space group	$P2_1/c$	$P\bar{1}$	$P2_1/n$
a/Å	6.8843(6)	8.9980(4)	9.7522(3)
b Å	11.6056(7)	9.0501(4)	12.2227(3)
c/Å	17.7118(10)	14.2542(6)	19.9917(5)
α/°	90	107.851(4)	90
β/°	94.244(6)	100.439(4)	93.683(3)
γ/°	90	100.556(4)	90
V/Å^3	1411.23(17)	1050.66(8)	2378.05(11)
Z	2	1	2
D_x/g cm^{-3}	2.082	1.854	1.689
μ/mm^{-1}	10.667	7.190	6.355
θ range/°	2.9–27.5	3.0–27.5	2.8–27.5
Reflections measured	15 284	12 872	26 714
Independent reflections; R_{int}	3218; 0.030	4751; 0.054	5408; 0.032
Reflections with $I > 2\sigma(I)$	2955	4433	4894
Number of parameters	149	254	254
$R(F)$ [$I > 2\sigma(I)$ reflections]	0.025	0.024	0.021
a, b in weight scheme	0.031, 3.103	0.008, 0	0.010, 1.698
w$R(F^2)$ (all data)	0.064	0.044	0.041
GOF(F^2)	1.08	0.97	1.05
$\Delta\rho_{max,min}$ (e Å^{-3})	1.71, −1.46	1.12, −1.31	0.59, −0.61

aseptically placed on Mueller-Hinton agar surfaces and 5 μl of the dissolved compounds were immediately added to discs. DMSO was used as a negative control whereas standard antibiotic paper disc was used as the positive control. All plates were incubated at 37 °C for 24 h. The anti-bacterial activity was evaluated by measuring the diameter of the inhibition zone against the test bacterial strains. Each trial was performed in triplicate.

Minimum inhibitory concentration (MIC) and minimum bactericidal concentration (MBC) determination. The MIC was determined by the broth micro-dilution method according to the NCCLS guidelines. An inoculum suspension with a density 10^5 CFU ml^{-1} of exponentially growing bacterial cells was added into each well. The test compounds were serially two-fold diluted in DMSO and then added to each well of a 96-well microplate. The 96-well microplates were incubated at 37 °C for 24 h. All tests were performed in triplicate. Four controls comprising medium with standard anti-biotic (positive control), medium with DMSO (solvent control), medium with inoculum bacterial cells (negative control) and medium with broth only (negative growth control) were included in each test. The bacterial growth was detected by adding 50 μl of a 0.2 mg ml^{-1} *p*-iodonitrotetrazolium violet (INT) indicator solution into each of the microplate wells and incubated at 37 °C for 30 min. under aerobic agitation. The INT changed from clear to red in the presence of bacterial activity. Where bacterial growth was inhibited, the suspension in the well remained clear after incubation with INT. The lowest concentration of the tested compound which completely inhibited bacterial growth was taken as the MIC. After MIC determination of each tested compound, an aliquot of 100 μl from each well which showed no visible growth was spread onto MHA at 37 °C for 24 h. The MBC is defined as the lowest concentration of the tested compound at which bacteria are killed.

Results and discussion

Syntheses and spectroscopy

The reaction of *p*-phenylene di-isothiocyanate with MeOH in the presence of base yielded bipodal LH_2 in high yield. The ^{1}H and, especially, ^{13}C NMR of LH_2 showed unexpected features in that chemically equivalent sites gave multiple resonances. Accordingly, a variable temperature ^{1}H NMR study in DMSO-d_6 solution (to attain a wider temperature range) was conducted with the results summarised in Table 2. Two resonances were observed for the ring protons when equivalence might have been expected. The splitting is ascribed to the formation of intramolecular methyl-C–H$\cdots\pi$(aryl) interactions rendering the protons

Table 2 Variable temperature ^{1}H NMR data (δ, ppm; $W_{1/2}$, band width at half-height) for LH_2 recorded in DMSO-d_6 solution

Temp. (°C)	NH	aryl-H	Ome	$W_{1/2}$ (Hz)
28	11.08	7.59, 7.29	3.98	29.32
38	11.04	7.57, 7.31	3.98	12.40
48	10.99	7.41	3.98	6.52
58	10.95	7.44	3.99	4.95
68	10.90	7.44	3.99 (sh, 3.98)	3.17
78	10.86	7.44	4.00 (sh, 3.98)	2.29

inequivalent. Upon heating the solution, the two signals coalesced into a single resonance, most likely due to rapid exchange, ESI Fig. S2a.† While no splitting was observed for the resonance due to the methyl protons, marked sharpening of the signal was evident as manifested in the $W_{1/2}$ values of 29.32 Hz at 28 °C *cf.* 2.29 Hz at 78 °C, indicative of a rapid exchange process, ESI Fig. S2b.† This was accompanied by a small downfield shift. The N-bound proton shifted upfield with increasing temperature consistent with reduced hydrogen bonding with the solvent. Evidence that the reduction in hydrogen bonding was a two-step process was found in the appearance of a shoulder for the methyl-proton at 68 °C consistent with the appearance of a minor, new species. The two environments arise at high temperature as one N-bound proton is involved in hydrogen bonding with the solvent and the other is not, *cf.* both participating in hydrogen bonding at low temperature.

Upon deprotonation and coordination of LH_2, the ^{1}H NMR resonance at 8.32 ($CDCl_3$) ascribed to N–H no longer persists in the spectra of **1–3**. By contrast to the spectrum recorded for LH_2, all chemically equivalent nuclei resonated at the same field strength. Also noteworthy are the significant upfield shifts in the resonances due to aryl-H of the central ring, *i.e.* to 6.72, 6.41 and 6.84 for **1–3**, respectively *cf.* 7.56 and 7.22 observed for LH_2. This observation is correlated with the presence of intramolecular Au$\cdots\pi$(aryl) interactions as delineated by X-ray crystallography (see below). The key finding of the $^{13}C\{^1H\}$ NMR spectra was that the four phenyl hydrogen-bearing nuclei, *ortho* and *meta*, are equivalent and appear as a single resonance in $CDCl_3$ solution. Similarly, the quaternary *ipso* carbons are also equivalent. In the ^{31}P NMR, a single resonance was observed for **1–3** at 35.6, 38.1 and 56.5, respectively, which are deshielded with respect to the uncoordinated Et_3P (−20.0), Ph_3P (−5.2) and Cy_3P (9.2) molecules measured under the same conditions. The relaxation attributes of **1**, being representative of the series, were also investigated.

In the $^{13}C\{^1H\}$ NMR spectrum of **1**, the *ortho* and *meta* carbons of the central ring resonated at $\delta = 122.84$ ppm. At 20 °C in $CDCl_3$ solution, the observed ^{13}C spin-lattice relaxation time (T_1) for this resonance was 0.69 s, and the NOE = 2.88; the NOE enhancement factor, η, was 1.88. As this η value is very near the maximum value of 1.988 for a ^{13}C nucleus, the dominant relaxation mechanism is the dipole–dipole relaxation mechanism (T_1^{dd}), for which the rate of this dipolar relaxation ($1/T_1^{dd}$), is proportional to the correlation time.[12,25] The observed T_1 is very low for phenyl nuclei in solution and is consistent with very low mobility of the phenyl group in the molecule. Hence, the observed ^{13}C relaxation data are consistent with severe hindrance in the internal rotation of the phenyl group.

The IR spectra of compounds **1–3** confirmed the absence of broad absorption at 3219 cm^{-1}, due to ν(N–H) in LH_2. Further, the red shifts of the ν(C–N) absorption to ~1400 cm^{-1}, and blue shifts of ν(C=S) to ~1100 cm^{-1} in **1–3** when compared to LH_2 provide further evidence for complexation.

Crystallography

The crystal structures of **1–3** were established by X-ray crystallography: the molecular structures are shown in Fig. 1 and selected geometric parameters are collated in Table 3. The molecule in **1**, Fig. 1a, is located about a centre of inversion and features a linear gold atom geometry defined by the phosphane-P and thiolate-S atoms. As usual for this type of structure,[6] the Au–S bond length is longer than that of Au–P. As the crystal

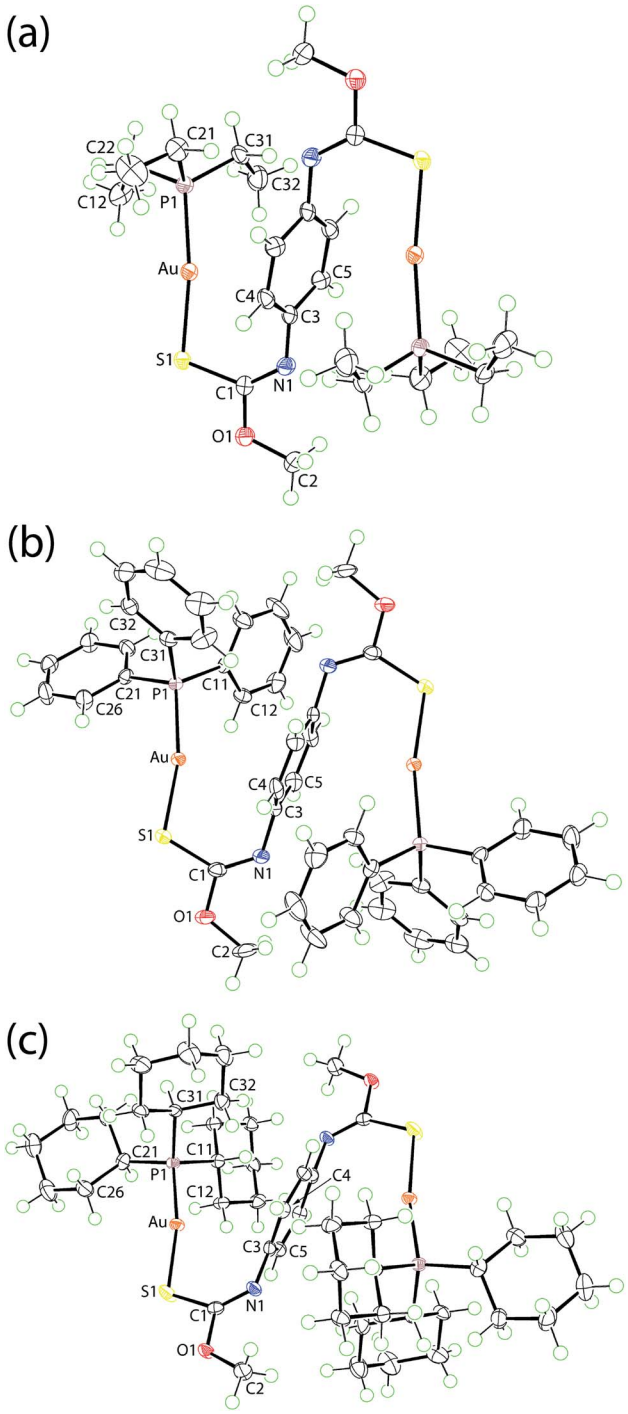

Fig. 1 Perspective views of the molecules of (a) **1**, (b) **2** and (c) **3**. Displacement ellipsoids are drawn at the 70% probability level and hydrogen atoms are shown as small spheres of arbitrary radii. The unlabelled atoms in (a) are related by the symmetry operation $1 - x$, $2 - y$, $-z$, and in (b) and (c) by $1 - x$, $1 - y$, $-z$.

Table 3 Selected bond lengths (Å) and angles (°) for **1–3**

	1	2	3
Au–S1	2.3152(10)	2.3058(9)	2.3019(6)
Au–P1	2.2663(10)	2.2593(9)	2.2695(6)
C1–S1	1.762(4)	1.761(3)	1.756(3)
C1–O1	1.372(5)	1.356(4)	1.362(3)
C1–N1	1.258(5)	1.268(4)	1.263(3)
S1–Au–P1	172.13(4)	167.79(3)	168.63(2)
Au–S1–C1	107.07(14)	107.37(12)	111.77(9)
C1–N1–C3	123.5(4)	122.3(3)	124.8(2)
S1–C1–O1	108.5(3)	108.1(2)	106.82(17)
S1–C1–N1	132.8(3)	131.3(3)	134.3(2)
O1–C1–N1	118.7(4)	120.6(3)	118.8(2)
Au···Cg(aryl)[a]	3.26	3.32	3.55
α[a]	22.7	21.6	30.7

[a] α is the angle between the normal to the plane through the central ring and the vector passing through the centroid (Cg) of the aryl ring to the Au atom.

structure of the precursor thiocarbamide, LH_2, is not available, the comparison between the geometric parameters defining the thiolate ligand in **1** will be made with PhN(H)C(=S)OMe.[26] The most notable observations is the elongation of the C1–S1 and contraction of the C1–N1 bond lengths in **1**, Table 1, compared with 1.6708(11) and 1.3288(15) Å, respectively in the uncoordinated molecule.[26] These changes are consistent with L^{2-} coordinating each gold atom as a thiolate ligand. The rearrangement of electron density in the anion also results in significant differences in bond angles whereby the S1–C1–O1 angle has contracted by about 16°, and the S1–C1–N1 and O1–C1–N1 angles have expanded by about 10 and 6°, respectively, observations readily correlated with the increased electron density in the C1–N1 bond. The molecular structures of **2** and **3** have essentially the same features as described for **1**, as highlighted in the overlay diagram shown in Fig. 2 that shows only small conformational variations. According to a search of the Cambridge Structural Database (CSD),[27] there are no precedents for binuclear structures based on bipodal thiocarbamates or analogues of higher denticity.

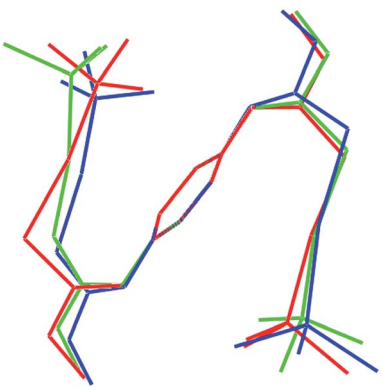

Fig. 2 Overlay diagram of **1** (red image), **2** (green) and **3** (blue). No hydrogen atoms are shown and only the α-carbon atoms of the phosphane ligands are included. The molecules have been overlapped so that the central rings are coincident.

The crystal packing of **1** is devoid of directional intermolecular interactions and may be described as comprising columns of molecules parallel to the *a*-axis, ESI Fig. S3a.† Weak C–H···π(aryl) interactions are noted in the crystal packing of **2**, and methylene-C–H···O contacts are seen in **3**. Despite these and the disparity in space groups, Table 1, the packing for each of **2** and **3** is as described for **1**, *i.e.* comprising columns of molecules aligned along the *a*-axis, ESI Fig. S3b and c.†

The linear coordination geometries for gold deviate by up to 12° from the ideal, deviations that are ascribed to the presence of intramolecular Au···π(aryl) interactions, Table 3. Such deviations are usually observed in related mononuclear structures of $[MeOC(S)=NR]^-$ but more often than not due to intramolecular Au···O interactions. Indeed, of the 31 structures available in the CSD[27] with the general formula, $R_3PAu[SC(OMe)=NR']$, and diphosphane analogues,[6a,28] 27 feature Au···O interactions in the range 2.862(3) Å for R = Ph & R′ = *p*-tol,[6c] to 3.172(8) Å for R = Cy & R′ = *p*-NO_2Ph.[6a] The remaining structures, each with isomeric tol_3P ligands, were reported to form intramolecular Au···π(aryl) interactions in the absence of steric hindrance and by judicious combinations of R and R′ groups.[6c] Given that in no circumstances were intramolecular Au···π(aryl) interactions formed for R_3P ligands with R = Et, Ph or Cy, the observation of these interactions in **1–3** was unexpected. The fickle nature of the formation of Au···π(aryl) interactions is probably best illustrated in the polymorphs of $dppm(AuCl)_2$ where in one form, an intramolecular Au···Au interaction is formed within an A-frame arrangement,[29a] whereas in the other polymorph, an intramolecular Au···π(aryl) interaction was observed instead.[29b] In order to probe further the nature of the Au···π(aryl) interactions formed in **1–3**, **1** was subjected to a computational study.

Optimised molecular structures

Phosphanegold(I) thiolates sometimes present unexpected structures.[30] For example, in structures of the type $R_3PAu[SC(=S)OR']$, R,R′ = alkyl/aryl, intramolecular Au···O interactions are usually formed giving rise to compact structures, rather than the intramolecular Au···S contacts expected from hard acid/soft base considerations. The latter interactions lead to open, rod-like molecular structures.[30a–c] In a similar vein, in a related species, *i.e.* $Cy_3PAu[SC_6H_4$-2-$CO_2H]$, in one polymorph the anticipated eight-membered $\{...HOCO\}_2$ synthon is formed, linking molecules in the crystal structure to form rod-type conformations. However, in each of the three other polymorphs, intramolecular O–H···S(thiolate) hydrogen bonds are formed instead, leading to spherical molecules.[30d,e] The unexpected structures were rationalised in terms of global crystal packing considerations,[31] in that the packing of spherical aggregates is more efficient that the packing of "rods".[30]

Geometry optimisation calculations were performed on **1** with the energy minimised structure having a conformation very similar to the experimentally observed structure. As highlighted in Fig. 3, there has been a flattening in the N=C–S–Au part of the

geometry optimised molecule as manifested in the N1–C1–S1–Au dihedral angle of −0.9°, *cf.* 14.8(5)° in the experimental structure. Conformational differences are also noted in the phosphane-bound ethyl groups. Further, the calculations show that the conformation presenting two intramolecular Au···π(aryl) contacts, as is experimentally observed in the crystal structure of **1**, is more stable by 12.2 kcal mol^{-1} with respect to the conformation featuring one Au···π(aryl) contact and one Au···O contact, and by 23.6 kcal mol^{-1} than the rod-like conformer with two Au···O interactions, Fig. 4. These results shown the Au···π(aryl) interaction is much stronger than Au···O, and roughly additive.

The Bader delocalization indices (DI's)[32] were calculated at the LC-ωPBE-XDM level between gold and the rest of the atoms in the three studied conformations. Intermolecular DI's are an excellent tool to evaluate the degree of electron delocalization (charge transfer) between interacting fragments.[33] For the conformations featuring Au···π(aryl) interactions, there is a significant amount of electron sharing between the gold atoms and the central ring, indicating the existence of orbital interactions between the gold atom and the π-system, and justifying the high stability of this contact, Fig. 4. The DI between the two gold atoms and the aryl ring is 0.56 in the compact conformer and 0.29 in the mixed Au···π(aryl)/Au···O conformer. The degree of electron delocalization between Au and the thiocarbamate-O atom in the Au···O contact is relatively small in comparison (0.10), although larger than the DI with the atoms adjacent to the oxygen, which indicates an interaction weaker than Au···π(aryl), in agreement with the energies. In addition, the S–Au–P angle is linear for the Au···O contact but bends slightly (170°) when a Au···π(aryl) contact is present, indicating a steric clash between the P-bound ethyl groups and the central ring. Despite this steric clash, the large stabilization caused by electron delocalization across the intramolecular Au···π(aryl) contact is clearly responsible for the conformation adopted in the crystal structure.

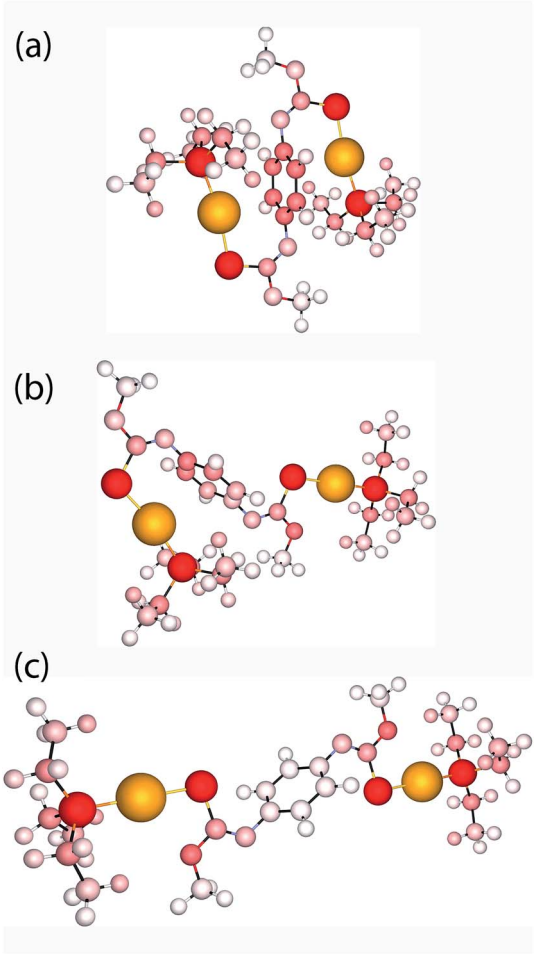

Fig. 4 Calculated structures for **1**: (a) the compact, spherical, conformation with two intramolecular Au···π(aryl) interactions, (b) intermediate structure with one Au···π(aryl) and one Au···O contact, and (c) the open, rod-like, conformation with two Au···O interactions. Bader's delocalization indices between gold (in orange) and all other individual atoms are given as a colour scale ranging from zero (white) to 0.30 (red).

Thermogravimetric analysis

Traces for the thermogravimetric analysis for **1–3** are given in ESI Fig. S4.† The decomposition pathways are quite similar for **1–3** and the following sequence is proposed. For **1**, three discernible steps were resolved: step 1 – onset temperature 181.9 °C to end 226.9 °C resulted in a weight loss of 73.3% *cf.* 70.7% corresponding to the loss of 2Et_3P. The second step (226.9–441.8 °C) saw a weight loss of 18.0% *cf.* 21.5%, correlated with loss of (2L–2S) leaving 2AuS (obs., calcd weight remaining 52.7% *cf.* 51.8%). The final step (441.8–806.1 °C) correlated with a weight loss of 7.2% *cf.* 7.3% expected for the loss of 2S with 2Au remaining (obs., calcd weight remaining 45.4% *cf.* 44.5%). The difference between the decomposition pathway for **1** and those for **2** and **3** is that there is no clear distinction between the first two steps for **2** and **3**. Thus, for **2**, step 1, between 163.5 and 346.7 °C, is accompanied by a weight loss of 55.2% *cf.* with 60.9% for the concomitant loss calculated for 2Ph_3P and (2L–2S) (obs., calcd weight remaining for 2AuS 44.7% *cf.* 39.1%), and step 2, between 346.7 and 815.2 °C, having a weight loss of 9.8% *cf.* with the theoretical value of 5.5% expected for the loss of 2S leaving Au (obs., calcd weight remaining for 2Au 35.0%

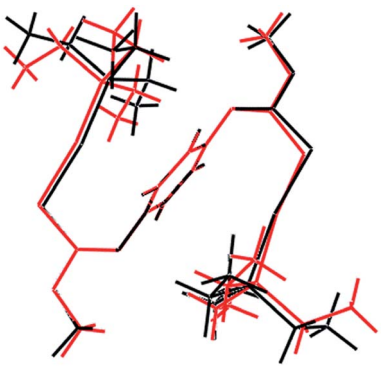

Fig. 3 Overlay diagram of the experimental molecular structure of **1** (red image) and the energy minimised structure (black). The molecules have been overlapped so that the central rings are coincident.

cf. 33.6%). The values for step 1 in the decomposition of **3** are onset-end temperatures 160.7 and 422.6 °C with 62.7% weight loss *cf.* with calculated 62.1% for the loss $2Cy_3P$ and (2L–2S) (obs., calcd weight remaining for 2AuS 37.2% *cf.* 37.8%), and for step 2, 422.6 to 815.2 °C with 3.6% weight loss *cf.* with calculated 5.3% for the loss 2S (obs., calcd weight remaining for 2Au 33.6% *cf.* 32.6%).

Evaluation of anti-bacterial activity

A total of 24 strains of pathogen were screened in the present study, and the results of the disk diffusion assay are presented in the Table 4. Compounds **1–3** exhibited variable degrees of anti-bacterial activity against the clinically important pathogens tested; LH_2 showed no inhibitory activity toward the tested bacteria. Of the series, **1** was the most active compound with complete inhibitory activity against all tested Gram-positive and Gram-negative pathogens, except *P. aeruginosa*, which is only partially inhibited by **1**. A partial zone of inhibition is defined as incomplete inhibition of bacterial growth and the formation of a film of bacteria on the surface agar. The Gram-positive bacteria were most susceptible toward **1**, with greater inhibition zones, ranging from 18 to 30 mm, compared with Gram-negative bacteria, with reduced inhibition zones, ranging from 7 to 23 mm. Mild anti-bacterial activities against several Gram-positive bacteria were observed for **2** and **3**, with clear zones of inhibition ranging from 7 to 10 mm. Compound **2** was active against all the tested Gram-positive bacteria except *B. cereus*. By contrast, **3** exhibited the lowest activity of the series, being potent in only five of eight strains of Gram-positive bacteria, *i.e*. *B. subtilis, E. faecium*, *L. monocytogenes*, MRSA and *S. saprophyticus.* Clearly, in this preliminary anti-bacterial assay, the tested Gram-positive bacteria are more susceptible than Gram-negative bacteria. This finding is also supported by studies which reported that Gram-negative bacteria are less susceptible to anti-microbial agents[34] and is consistent with results obtained recently for mononcuclear phosphanegold(I) analogues.[11] The presence of the outer lipopolysaccharide layer in Gram-negative bacteria inhibits the access of most drugs to intracellular targets in bacteria and renders Gram-negative bacteria less susceptible to drugs than Gram-positive bacteria, which lack an outer membrane.[35]

Using the broth micro-dilution method, the anti-bacterial sensitivity of **1–3** was quantitatively assessed by determining the minimum inhibitory concentration (MIC), defined as the highest dilution at which no bacterial growth was detected, Table 5. A lower MIC value indicates a better anti-microbial agent as a smaller amount of trial compound is required to inhibit bacterial growth. Compound **1** exhibited excellent inhibitory activity toward all susceptible Gram-positive bacteria compared with **2** and **3**, and standard anti-biotics

Table 4 Anti-bacterial activity measured by zone of inhibition (mm) of **1–3**, LH_2 and standard anti-biotics[c]

Microorganism	1	2	3	LH_2	Standard anti-biotics
Gram-positive bacteria					
B. cereus ATCC10876	22	—	—	—	11[a]
B. subtilis ATCC6633	27	10	8	—	24[a]
E. faecalis ATCC29212	20	9	—	—	11[a]
E. faecium ATCC19434	18	9	8	—	16[b]
L. monocytogenes ATCC19117	20	9	8	—	27[a]
S. aureus (MRSA) ATCC43300	23	9	7	—	14[b]
S. aureus ATCC25923	30	9	—	—	18[b]
S. saprophyticus ATCC15305	30	9	8	—	29[a]
Gram-negative bacteria					
A. baumannii ATCC19606	13	—	—	—	16[a]
A. hydrophilla ATCC35654	8	—	—	—	22[a]
C. freundii ATCC8090	8	—	—	—	26[a]
E. aerogenes ATCC13048	7	—	—	—	20[a]
E. cloacae ATCC35030	8	—	—	—	20[a]
E. coli ATCC25922	10	—	—	—	18[a]
K. pneumonia ATCC700603	8	—	—	—	13[a]
P. aeruginosa ATCC27853	14 (T)	—	—	—	14[a]
P. mirabilis ATCC25933	8	—	—	—	14[b]
P. vulgaris ATCC13315	14	—	—	—	19[b]
S. typhimurium ATCC14028	9	—	—	—	24[a]
*S. paratyphi*A ATCC9150	9	—	—	—	22[a]
S. flexneri ATCC12022	12	—	—	—	18[a]
S. sonnei ATCC9290	10	—	—	—	19[a]
S. maltophilia ATCC13637	9	—	—	—	23[b]
V. parahaemolyticus ATCC17802	23	—	—	—	30[a]

[a] Tetracycline. [b] Chloramphenicol. [c] The diameter of inhibition zones in millimetres (mm) were measured in the disc after 24 h incubation;—, no zone of inhibition; (*T*), partial zone of inhibition.

Table 5 MIC and MBC of **1–3**, LH_2 and standard anti-biotics against selected Gram-positive and Gram-negative bacteria[c]

	1		**2**		**3**		Standard anti-biotics	
Microorganism	MIC	MBC/MIC	MIC	MBC/MIC	MIC	MBC/MIC	MIC	MBC/MIC
Gram-positive bacteria								
B. cereus ATCC10876	0.10	1	—	—	—	—	6.25[a]	1
B. subtilis ATCC6633	0.20	1	0.78	1	25.00	1	0.20[a]	1
E. faecalis ATCC29212	0.39	1	6.25	1	—	—	12.50[a]	1
E. faecium ATCC19434	0.20	32	3.13	4	6.25	4	12.50[b]	ND
L. monocytogenes ATCC19117	0.10	1	1.56	1	6.25	1	12.50[a]	1
S. aureus (MRSA) ATCC43300	0.10	2	1.56	1	50.00	1	12.50[b]	1
S. aureus ATCC25923	0.10	2	3.13	1	—	—	12.50[b]	1
S. saprophyticus ATCC15305	0.10	2	1.56	1	6.25	2	0.39[a]	ND
Gram-negative bacteria								
A. baumannii ATCC19606	6.25	1	—	—	—	—	0.39[a]	32
A. hydrophilla ATCC35654	6.25	2	—	—	—	—	0.39[a]	1
C. freundii ATCC8090	25.00	4	—	—	—	—	0.78[a]	32
E. aerogenes ATCC13048	25.00	4	—	—	—	—	1.56[a]	32
E. cloacae ATCC35030	25.00	1	—	—	—	—	1.56[a]	ND
E. coli ATCC25922	12.50	1	—	—	—	—	0.39[a]	ND
K. pneumoniae ATCC700603	50.00	ND	—	—	—	—	12.50[a]	ND
P. aeruginosa ATCC27853	—	—	—	—	—	—	6.25[a]	ND
P. mirabilis ATCC25933	12.50	2	—	—	—	—	12.50[b]	8
P. vulgaris ATCC13315	3.13	4	—	—	—	—	12.50[b]	4
S. typhimurium ATCC14028	12.50	1	—	—	—	—	1.56[a]	32
S. paratyphi a ATCC9150	12.50	1	—	—	—	—	1.56[a]	32
S. flexneri ATCC12022	6.25	1	—	—	—	—	0.78[a]	32
S. sonnei ATCC9290	6.25	2	—	—	—	—	0.78[a]	32
S. maltophilia ATCC13637	3.13	4	—	—	—	—	3.13[b]	ND
V. parahaemolyticus ATCC17802	1.56	1	—	—	—	—	0.10[a]	1

[a] Tetracycline. [b] Chloramphenicol. [c] MIC – minimum inhibitory concentration (μg ml^{-1}); MBC/MIC ratio for bacteriostatic or bactericidal activity; – not applicable; ND – not determined as the bacterium had grown across all tested dilution (MBC > 100 μg ml^{-1}).

(tetracycline and chloramphenicol), with lowest MIC values in the range 0.10–0.39 μg ml^{-1}. The most susceptible Gram-positive bacteria strains toward **1** were *B. cereus*, *L. monocytogenes*, MRSA, *S. aureus* and *S. saprophyticus* (MIC's = 0.10 μg ml^{-1}) follow by *B. subtilis* and *E. faecium* (MIC's = 0.20 μg ml^{-1}) and *E. faecalis* (MIC = 0.39 μg ml^{-1}). However, tetracycline and chloramphenicol showed equal or, normally, greater anti-bacterial activity toward Gram-negative bacteria compared to **1**, with lower MIC values in the range 0.10–12.5 μg ml^{-1}. Compound **2** exhibited more promising MIC values (0.78–6.25 μg ml^{-1}) than **3** (6.25–50.00 μg ml^{-1}) toward susceptible Gram-positive bacteria. In addition, **2** displayed greater activity compared with tetracycline and chloramphenicol against *E. faecalis*, *E. faecium*, *L. monocytogenes*, MRSA and *S. aureus*, with lower MIC values in the range 1.56–6.25 μg ml^{-1}.

The zone of inhibition and MIC tests may reflect temporary inhibition of bacterial growth (bacteriostatic) or bacterial killing (bactericidal) by a test compound. The bactericidal properties of **1–3** against susceptible strains were further analyzed by the minimum bactericidal concentration (MBC) assay and summarized as MBC/MIC ratios in Table 5. An anti-microbial agent is bactericidal if the MBC is not more than fourfold higher than the MIC, *i.e.* MBC/MIC ≤ 4. By contrast, the anti-microbial agent is bacteriostatic if the MBC is more than four-fold greater than the MIC, *i.e.* MBC/MIC ≤ 4.[36] Compounds **2** and **3** were shown to be bactericidal (MBC/MIC ≤ 4) toward the susceptible Gram-positive bacteria strains. For **1**, bactericidal activity was observed against all susceptible Gram-positive and Gram-negative bacteria with the exception of *E. faecium* (MBC/MIC = 32) and *K. pneumoniae* (MBC/MIC = ND). These results suggest that **1–3** are considered bactericidal agents but the activity of **1** is dependent on the specific bacterial strain.

The broad spectrum of activity exhibited by **1** (R = Et) against Gram-positive and Gram-negative bacteria, and the specific activity against Gram-positive bacteria exhibited by **2** and **3** suggests a key role for the phosphane ligand. This is vindication of an earlier study against the same panel of 24 pathogens but where the thiolate was a dithiocarbamate ligand, *i.e.* $R_3PAu[S_2CN(iPr)CH_2CH_2OH]$, for R = Et, Ph and Cy.[37] In this study a similar observation was made in that the R = Et derivative had broad range activity against both Gram-positive and Gram-negative bacteria, and the activity of the R = Ph and Cy species was limited to Gram-positive bacteria.[37] Perhaps once thought as being too expensive for development as anti-microbial agents, the emerging resistance to conventional therapies suggest that gold compounds may play a clinical role, especially against virulent strains of bacteria such as MRSA.

Conclusions

Three new binuclear phospanegold(I) compounds of a bipodal ligand have been characterised. Crystallography shows the uniform adoption of a spherical aggregate featuring unexpected intramolecular Au···π(aryl) interactions. Theory shows these interactions to be attractive, providing energies of stabilization to the molecular structure of **1** greater than 12 kcal mol^{-1} compared to putative Au···O interactions. Compounds **1–3** exhibited, predominantly, a bactericidal effect on Gram-positive (**1–3**) and Gram-negative (only **1**) pathogens, with **1** perhaps having potential clinical benefits over standard anti-biotics in bacteriostatic therapy for immune-compromised patients, *i.e.* with cancer and neutropenia, by prompt elimination of the pathogen to therefore reduce the likelihood of the spread of infection.

Acknowledgements

Support from the Ministry of Higher Education, Malaysia, and the University of Malaya, for High Impact Research grant (UM.C/HIR-MOHE/SC/12) is gratefully acknowledged. AOR acknowledges support from the Spanish Malta/Consolider initiative (no. CSD2007-00045) and the Alberta Innovates Technology Futures (AITF) for funding.

References

1 *e.g.* S. S. Pathaneni and G. R. Desiraju, *J. Chem. Soc., Dalton Trans.*, 1993, 319; M. J. Katz, K. Sakai and D. B. Leznoff, *Chem. Soc. Rev.*, 2008, **37**, 1884; H. Schmidbaur and A. Schier, *Chem. Soc. Rev.*, 2008, **37**, 1931; H. E. Abdou, A. A. Mohamed, J. P. Fackler, A. Burini, R. Galassi, J. M. Lopez-de-Luzuriaga and M. E. Olmos, *Coord. Chem. Rev.*, 2009, **253**, 1661; H. Schmidbaur and A. Schier, *Chem. Soc. Rev.*, 2012, **41**, 370; E. R. T. Tiekink, *Coord. Chem. Rev.*, 2014, **275**, 130.

2 P. Pyykkö and Y.-F. Zhao, *Angew. Chem., Int. Ed. Engl.*, 1991, **30**, 604; P. Pyykkö, *Inorg. Chim. Acta*, 2005, **358**, 4113; H. Schmidbaur and A. Schier, *Chem. Soc. Rev.*, 2008, **37**, 1931; S. Sculforta and P. Braunstein, *Chem. Soc. Rev.*, 2011, **40**, 2741.

3 *e.g.* A. L. Balch, *Struct. Bonding*, 2007, **123**, 1; V. W.-W. Yam and E. C.-C. Cheng, *Top. Curr. Chem.*, 2007, **281**, 269; E. R. T. Tiekink and J.-G. Kang, *Coord. Chem. Rev.*, 2009, **253**, 1627; X. He and V. W.-W. Yam, *Coord. Chem. Rev.*, 2011, **255**, 2111; E. E. Langdon-Jones and S. J. A. Pope, *Chem. Commun.*, 2014, **50**, 10343.

4 (*a*) I. Caracelli, J. Zukerman-Schpector and E. R. T. Tiekink, *Gold Bull.*, 2013, **46**, 81; (*b*) J. Zukerman-Schpector and E. R. T. Tiekink, *CrystEngComm*, 2009, **11**, 1176; (*c*) E. R. T. Tiekink and J. Zukerman-Schpector, *CrystEngComm*, 2009, **11**, 2701.

5 *e.g.* (*a*) B. K. Min and C. M. Friend, *Chem. Rev.*, 2007, **107**, 2709; (*b*) T. Takei, T. Akita, I. Nakamura, T. Fujitani, M. Okumura, K. Okazaki, J. H. Huang, T. Ishida and M. Haruta, *Adv. Catal.*, 2012, **55**, 1; (*c*) M. Pan, J. L. Gong, G. B. Dong and C. B. Mullins, *Acc. Chem. Res.*, 2014, **47**, 750.

6 (*a*) S. Y. Ho, E. C.-C. Cheng, E. R. T. Tiekink and V. W.-W. Yam, *Inorg. Chem.*, 2006, **45**, 8165; (*b*) S. Y. Ho and E. R. T. Tiekink, *CrystEngComm*, 2007, **9**, 368; (*c*) F. S. Kuan, S. Y. Ho, P. P. Tadbuppa and E. R. T. Tiekink, *CrystEngComm*, 2008, **10**, 548.

7 (*a*) S. J. Berners-Price and A. Filipovska, *Metallomics*, 2011, **3**, 863; (*b*) W. F. Kean and I. R. L. Kean, *Inflammopharmacology*, 2008, **16**, 112; (*c*) E. R. T. Tiekink, *Gold Bull.*, 2003, **36**, 117; (*d*) J. F. Fries, D. Bloch, P. Spitz and D. M. Mitchell, *Am. J. Med.*, 1985, **78**, 56.

8 E. R. T. Tiekink, *Critical Reviews in Oncology/Hematology*, 2002, **42**, 225; I. Ott, *Coord. Chem. Rev.*, 2009, **253**, 1670; C. Gabbiani, M. A. Cinellu, L. Maiore, L. Massai, F. Scaletti and L. Messori, *Inorg. Chim. Acta*, 2012, **393**, 115; N. Cutillas, G. S. Yellol, C. de Haro, C. Vicente, V. Rodriguez and J. Ruiz, *Coord. Chem. Rev.*, 2013, **257**, 2784; C. Nardon, S. M. Schmitt, H. J. Yang, J. Zuo, D. Fregona and Q. P. Dou, *PLoS One*, 2014, **9**, e84248; B. Bertrand and A. Casini, *Dalton Trans.*, 2014, 4209.

9 C. I. Yeo, K. K. Ooi, A. Md Akim, K. P. Ang, Z. A. Fairuz, S. N. B. A. Halim, S. W. Ng, H.-L. Seng and E. R. T. Tiekink, *J. Inorg. Biochem.*, 2013, **127**, 24.

10 B. Đ. Glišić and M. I. Djuran, *Dalton Trans.*, 2014, 5950.

11 C. I. Yeo, J.-H. Sim, C.-H. Khoo, Z.-J. Goh, K.-P. Ang, Y.-K. Cheah, Z. A. Fairuz, S. N. B. A. Halim, S. W. Ng, H.-L. Seng and E. R. T. Tiekink, *Gold Bull.*, 2013, **46**, 145.

12 R. K. Harris, *Nuclear Magnetic Resonance Spectroscopy*, Longman, Harlow, 1986.

13 *X'Pert HighScore Plus*, ed. B. V. Almelo, PANalytical, The Netherlands, 2009.

14 (*a*) V. J. Hall, G. Siasios and E. R. T. Tiekink, *Aust. J. Chem.*, 1993, **46**, 561; (*b*) S. Y. Ho, R. P. A. Bettens, D. Dakternieks, A. Duthie and E. R. T. Tiekink, *CrystEngComm*, 2005, **7**, 682; (*c*) F. S. Kuan, F. Mohr, P. P. Tadbuppa and E. R. T. Tiekink, *CrystEngComm*, 2007, **9**, 574.

15 (*a*) *CrysAlisPro*, Agilent Technologies, Santa Clara, CA, USA, 2014; (*b*) G. M. Sheldrick, *Acta Crystallogr., Sect. A: Found. Crystallogr.*, 2008, **64**, 112; (*c*) L. J. Farrugia, *J. Appl. Crystallogr.*, 2012, **45**, 849; (*d*) A. L. Spek, *Acta Crystallogr., Sect. D: Biol. Crystallogr.*, 2009, **65**, 148; (*e*) *DIAMOND, Visual Crystal Structure Information System, Version 3.1, CRYSTAL IMPACT*, Postfach 1251, D-53002 Bonn, Germany, 2006; (*f*) J. Gans and D. Shalloway, *J. Mol. Graphics Modell.*, 2001, **19**, 557.

16 M. J. Frisch, G. W. Trucks, H. B. Schlegel, G. E. Scuseria, M. A. Robb, J. R. Cheeseman, G. Scalmani, V. Barone, B. Mennucci, G. A. Petersson, H. Nakatsuji, M. Caricato, X. Li, H. P. Hratchian, A. F. Izmaylov, J. Bloino, G. Zheng, J. L. Sonnenberg, M. Hada, M. Ehara, K. Toyota, R. Fukuda, J. Hasegawa, M. Ishida, T. Nakajima, Y. Honda, O. Kitao, H. Nakai, T. Vreven, J. A. Montgomery Jr, J. E. Peralta, F. Ogliaro, M. Bearpark, J. J. Heyd, E. Brothers, K. N. Kudin, V. N. Staroverov, R. Kobayashi, J. Normand, K. Raghavachari, A. Rendell, J. C. Burant, S. S. Iyengar, J. Tomasi, M. Cossi, N. Rega, J. M. Millam,

M. Klene, J. E. Knox, J. B. Cross, V. Bakken, C. Adamo, J. Jaramillo, R. Gomperts, R. E. Stratmann, O. Yazyev, A. J. Austin, R. Cammi, C. Pomelli, J. W. Ochterski, R. L. Martin, K. Morokuma, V. G. Zakrzewski, G. A. Voth, P. Salvador, J. J. Dannenberg, S. Dapprich, A. D. Daniels, Ö. Farkas, J. B. Foresman, J. V. Ortiz, J. Cioslowski and D. J. Fox, *Gaussian 09, Revision A.1*, Gaussian, Inc., Wallingford CT, 2009.

17 O. A. Vydrov and G. E. Scuseria, *J. Chem. Phys.*, 2006, **125**, 234109; O. A. Vydrov, J. Heyd, A. V. Krukau and G. E. Scuseria, *J. Chem. Phys.*, 2006, **125**, 074106.

18 A. D. Becke and E. R. Johnson, *J. Chem. Phys.*, 2007, **127**, 154108.

19 E. R. Johnson and A. D. Becke, *J. Chem. Phys.*, 2006, **124**, 174104.

20 A. Otero-de-la-Roza and E. R. Johnson, *J. Chem. Phys.*, 2013, **138**, 204109.

21 http://gatsby.ucmerced.edu/.

22 A. Otero-de-la-Roza, J. D. Mallory and E. R. Johnson, *J. Chem. Phys.*, 2014, **140**, 18A504.

23 K. A. Peterson and C. Puzzarini, *Theor. Chem. Acc.*, 2005, **114**, 283.

24 E. R. Johnson, A. Otero-de-la-Roza, S. G. Dale and G. A. DiLabio, *J. Chem. Phys.*, 2013, **139**, 214109.

25 S. Ng, F. M. Salleh, Y. Xie and H. F. Schaefer III, *J. Phys. Org. Chem.*, 2012, **25**, 1374.

26 S. Y. Ho, C. S. Lai and E. R. T. Tiekink, *Acta Crystallogr., Sect. E: Struct. Rep. Online*, 2003, **59**, o1155.

27 C. R. Groom and F. H. Allen, *Angew. Chem., Int. Ed.*, 2014, **53**, 662.

28 P. P. Tadbuppa and E. R. T. Tiekink, *Acta Crystallogr., Sect. E: Struct. Rep. Online*, 2007, **63**, m1101; P. P. Tadbuppa and E. R. T. Tiekink, *Acta Crystallogr., Sect. E: Struct. Rep. Online*, 2009, **65**, m1557; P. P. Tadbuppa and E. R. T. Tiekink, *Acta Crystallogr., Sect. E: Struct. Rep. Online*, 2009, **65**, m1558; P. P. Tadbuppa and E. R. T. Tiekink, *Acta Crystallogr., Sect. E: Struct. Rep. Online*, 2009, **65**, m1646; P. P. Tadbuppa and E. R. T. Tiekink, *Acta Crystallogr., Sect. E: Struct. Rep. Online*, 2009, **65**, m1700; P. P. Tadbuppa and E. R. T. Tiekink, *Acta Crystallogr., Sect. E: Struct. Rep. Online*, 2010, **66**, m450; P. P. Tadbuppa and E. R. T. Tiekink, *Acta Crystallogr., Sect. E: Struct. Rep. Online*, 2010, **66**, m664.

29 (*a*) H. Schmidbaur, A. Wohlleben, F. Wagner, O. Orama and G. Huttner, *Chem. Ber.*, 1977, **110**, 1748; (*b*) P. C. Healy, *Acta Crystallogr., Sect. E: Struct. Rep. Online*, 2003, **59**, m1112.

30 (*a*) G. Siasios and E. R. T. Tiekink, *Z. Kristallogr.*, 1993, **204**, 95; (*b*) G. Siasios and E. R. T. Tiekink, *Z. Kristallogr.*, 1993, **205**, 261; (*c*) E. R. T. Tiekink and I. Haiduc, *Prog. Inorg. Chem.*, 2005, **54**, 127; (*d*) P. D. Cookson and E. R. T. Tiekink, *J. Coord. Chem.*, 1992, **26**, 313; (*e*) D. R. Smyth, B. R. Vincent and E. R. T. Tiekink, *Cryst. Growth Des.*, 2001, **1**, 113.

31 J. D. Dunitz and A. Gavezzotti, *Acc. Chem. Res.*, 1999, **32**, 677; J. D. Dunitz and A. Gavezzotti, *Chem. Soc. Rev.*, 2009, **38**, 2622; J. D. Dunitz and A. Gavezzotti, *Cryst. Growth Des.*, 2012, **12**, 5873.

32 R. F. W. Bader and M. E. Stephens, *J. Am. Chem. Soc.*, 1975, **97**, 7391; R. F. W. Bader, A. Streitwieser, A. Neuhaus, K. E. Laidig and P. Speers, *J. Am. Chem. Soc.*, 1996, **118**, 4959.

33 A. Otero de la Roza, E. R. Johnson and G. A. DiLabio, *J. Chem. Theory Comput.*, 2014, **10**, 5436.

34 K. S. O. Ferraz, N. F. Saliva, J. G. D. Silva, L. F. D. Miranda, C. F. D. Romeiro, E. M. Souza-Fagundes, I. C. Mendes and H. Beraldo, *Eur. J. Med. Chem.*, 2012, **53**, 98.

35 P. Burn, *Trends Biochem. Sci.*, 1998, **13**, 79.

36 M. E. Levison, *Infect. Dis. Clin.*, 2004, **18**, 451.

37 J.-H. Sim, N. S. Jamaludin, C.-H. Khoo, Y.-K. Cheah, S. N. B. A. Halim, H.-L. Seng and E. R. T. Tiekink, *Gold Bull.*, 2014, **47**, 225.